Magnetoreflection spectroscopy of monolayer transition-metal dichalcogenide semiconductors in pulsed magnetic fields

Andreas V. Stier
National High Magnetic Field Laboratory, Los Alamos, New Mexico 87545

Kathleen M. McCreary and Berend T. Jonker
Materials Science and Technology Division, Naval Research Laboratory, Washington, DC 20375

Junichiro Kono
Department of Electrical and Computer Engineering, Department of Physics and Astronomy, and Department of Materials Science and NanoEngineering, Rice University, Houston, Texas 77005

Scott A. Crooker[a)]
National High Magnetic Field Laboratory, Los Alamos, New Mexico 87545

(Received 14 March 2016; accepted 26 April 2016; published 13 May 2016)

The authors describe recent experimental efforts to perform polarization-resolved optical spectroscopy of monolayer transition-metal dichalcogenide semiconductors in very large pulsed magnetic fields to 65 T. The experimental setup and technical challenges are discussed in detail, and temperature-dependent magnetoreflection spectra from atomically thin tungsten disulphide are presented. The data clearly reveal not only the valley Zeeman effect in these two-dimensional semiconductors but also the small quadratic exciton diamagnetic shift from which the very small exciton size can be directly inferred. Finally, the authors present model calculations that demonstrate how the measured diamagnetic shifts can be used to constrain estimates of the exciton binding energy in this new family of monolayer semiconductors. © *2016 American Vacuum Society*.
[http://dx.doi.org/10.1116/1.4948992]

I. INTRODUCTION

Historically, magneto-optical studies have played a central role in revealing the fundamental properties of excitons in bulk and low-dimensional semiconductors. Various polarization-resolved optical spectroscopies in applied magnetic fields have helped to determine the mass, size, energy, magnetic moment, and dimensionality of excitons and carriers in a great many conventional semiconductor materials.[1,2] Recently, a new family of atomically thin semiconductors known as the monolayer transition-metal dichalcogenides (TMDs) has captured the attention of physicists, materials scientists, and chemists working broadly in the fields of semiconductors and 2D materials.[3,4] These new monolayer TMDs, which include atomically thin flakes and films of MoS_2, $MoSe_2$, tungsten disulphide (WS_2), and WSe_2, are semiconductors possessing direct optical bandgaps at the K and K' points of their hexagonal Brillouin zone. Owing to strong spin–orbit coupling and their lack of structural inversion symmetry, spin and valley degrees of freedom are coupled and *valley-specific* optical selection rules exist for right- and left-circularly polarized light.[5,6] Consequently, a number of interesting optical and magneto-optical studies of these TMDs have been performed in recent years, in which both spin and valley physics were explored.[7–19]

On both theoretical and experimental grounds,[20–30] electron and hole masses in the monolayer TMDs are thought to be rather heavy (of order $0.5m_0$, where m_0 is the free electron mass), the exciton binding energies are reported to be extremely large (of order 500–1000 meV), and the physical sizes of the excitons are predicted to be very small (of order 1–2 nm). (In comparison, in GaAs the electron mass is $0.067m_0$, the exciton binding energy is only 4 meV, and the exciton Bohr radius is ∼20 nm.) For these reasons—and also because the photoluminescence and absorption linewidths in monolayer TMDs are relatively broad (∼10–40 meV, depending on the material)—very large magnetic fields of order 50–100 T are desirable so that the small Zeeman shifts and the even-smaller exciton diamagnetic shifts can be clearly resolved in the experimental data.

To this end, we have recently developed capabilities for performing polarization-resolved magnetoreflection studies of monolayer TMD materials at cryogenic temperatures down to 4 K, and in very high pulsed magnetic fields to 65 T. We recently reported the first results of such measurements (on monolayer MoS_2 and WS_2) in Ref. 19. The intent of this paper is therefore to present a considerably more detailed description of the experimental setup and of the challenges faced when working with monolayer materials in pulsed magnetic fields. In particular, we focus on how we achieve and verify the circular polarization selectivity, and how we mitigate problems due to the mechanical vibrations that are ubiquitous in pulsed-field studies. We present new data showing temperature-dependent studies of the valley Zeeman effect and exciton diamagnetic shift. Finally, we also extend recent calculations of the exciton binding energy in these monolayer TMDs to a more realistic case that includes the effect of the dielectric substrate, and discuss the experimental results within that context.

[a)]Electronic mail: crooker@lanl.gov

II. EXPERIMENT

A. Setup

Figure 1(a) shows one of the 65 T pulsed magnets used at the National High Magnetic Field Laboratory (NHMFL) at Los Alamos National Laboratory. The magnet has a 15 mm bore and is powered by a 16 kV, 32 mF capacitor bank. A liquid helium bath cryostat sits atop the magnet and has a long vacuum-insulated tail section that extends into the magnet bore. During operation, the magnet is immersed in liquid nitrogen to reduce its initial resistance. Full-field pulses can be repeated every 45 min, limited by the cool-down time of the magnet following each pulse. A representative field profile from this magnet is shown in Fig. 1(b). Magnetoreflectance studies were performed with the samples at cryogenic temperatures down to 4 K using a home-built fiber-coupled optical probe depicted in Fig. 1(c). The probe, which resides in an additional vacuum jacket filled with helium exchange gas, is constructed from nonmetallic fiberglass (G10) and polycarbonate materials (Vespel) and has a diameter of 8 mm.

Broadband white light from a xenon lamp was coupled to the samples using a 100 μm diameter multimode optical fiber. The light was focused onto the sample at near-normal incidence using a single aspheric lens (6 mm focal length, NA 0.3), and the reflected light was refocused by the same lens into a 600 μm diameter collection fiber. The collected light was dispersed in a 300 mm spectrometer and was detected with a liquid nitrogen cooled charge-coupled device (CCD) detector. The CCD was configured to acquire full spectra continuously at a rate of about 500 Hz (~2 ms/spectra) throughout the magnet pulse. The blue spikes in Fig. 1(b) show the CCD timing signal. The choice of 100 μm diameter for the delivery fiber achieves a satisfactory balance between the conflicting goals of achieving a small focused spot on the sample while still allowing a sufficient amount of light to be coupled from the xenon lamp to the sample.

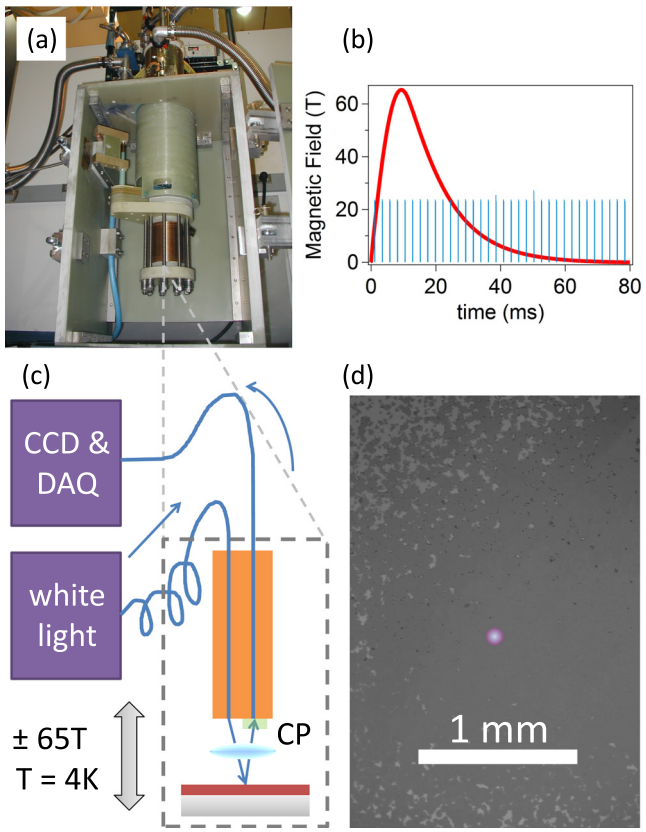

FIG. 1. (Color online) (a) Photograph of a 65 T capacitor-driven pulsed magnet at the NHMFL. The tail of a liquid helium bath cryostat extends down into the magnet bore. (b) Typical field profile (red curve). The blue spikes show the timing signal of the CCD; full 16-bit optical spectra are acquired at each spike. (c) Schematic of the fiber-coupled optical reflection probe. White light is coupled to the sample via a 100 μm diameter optical fiber and a single aspheric lens. CP = circular polarizer. Reflected light is refocused back into an adjacent 600 μm diameter collection fiber, and detected with a spectrometer and CCD. (d) Optical microscope image of a large-area WS_2 film grown by CVD on a Si/SiO_2 substrate. Dark (bright) regions show the monolayer WS_2 film (substrate). The spot size of the focused white light is ~100 μm as indicated by the red circle.

Polarization selectivity is achieved via a thin-film circular polarizer that can be mounted over either the delivery fiber or the collection fiber. Depending on the configuration and on the direction of the magnetic field (positive or negative), this provides sensitivity to the σ^+ or σ^- polarized optical transitions in the K or K' valleys of monolayer TMDs, as discussed in more detail below.

Figure 1(d) shows a typical image of the large-area monolayer WS_2 films used in these experiments. These films are grown by chemical vapor deposition (CVD) on Si/SiO_2 substrates and typically have millimeter-square regions with >99% monolayer coverage,[31] which is much larger than the ~100 μm diameter spot of the focused white light on the sample. Details of the sample growth and the characterization of film quality from photoluminescence and Raman spectroscopy can be found in Refs. 19 and 31.

The use of large-area CVD-grown films was critical for these pulsed magnetic field experiments. While stable optical alignment onto micron-scale exfoliated TMD flakes is relatively straightforward in low-field superconducting and dc magnets,[11–15] the mechanical vibrations inherent in pulsed magnets significantly complicate such approaches. Moreover, the *in situ* nanopositioners commonly used in dc magneto-spectroscopy of micron-scale samples are generally not amenable to the small bore sizes and rapidly varying magnetic field environment of a high-field pulsed magnet. These stringent alignment requirements are considerably relaxed, however, when using larger-area samples having high spatial uniformity because micron-scale vibrations and temperature drifts do not affect the detected signals to leading order. In this case, a fiber-coupled probe of the type described above typically suffices to obtain high quality spectra that are largely free from mechanical vibrations and subsequent misalignment during the magnet pulse. Similar fiber-coupled probe designs have been successfully used in conjunction with pulsed magnets to study millimeter-squared samples of magnetic semiconductors,[32,33] quantum wells,[34,35] colloidal quantum dots,[36,37] carbon nanotubes,[38,39] and polymers.[40]

B. Excitons in monolayer WS_2

Figure 2(a) shows the low-temperature reflection spectrum from a monolayer WS_2 film at zero magnetic field. The A and B exciton transitions are clearly visible. Their origin

can be understood from Fig. 2(b), which depicts the conduction and valence bands at the K and K' valleys, as well as the associated exciton transitions and optical selection rules. Strong spin–orbit coupling of the valence band splits the spin-up and spin-down components by ~400 meV in monolayer WS_2, giving rise to the large separation between the A and B exciton transitions. Owing to the valley-specific optical selection rules in these monolayer TMD materials, σ^+ circularly polarized light couples to both A and B exciton transitions in the K valley, while light of the opposite σ^- circular polarization couples to the exciton transitions in the K' valley.

At zero applied magnetic field, the bands and optical transitions in the K and K' valleys are nominally degenerate in energy and related by time-reversal symmetry. That is, spin-up conduction (valence) bands in K and spin-down conduction (valence) bands in K' have the same energy and equal-but-opposite total magnetic moment ($\boldsymbol{\mu}_K^{c,v} = -\boldsymbol{\mu}_{K'}^{c,v}$). Therefore, an applied magnetic field, which breaks time-reversal symmetry, will lift the K/K' valley degeneracy by shifting time-reversed pairs of states in opposite directions in accord with the Zeeman energy $-\boldsymbol{\mu} \cdot \mathbf{B}$. This will Zeeman-shift the measured exciton energy if the relevant conduction and the valence band moments are *unequal*: $\Delta E_Z = -(\boldsymbol{\mu}^c - \boldsymbol{\mu}^v) \cdot \mathbf{B}$.

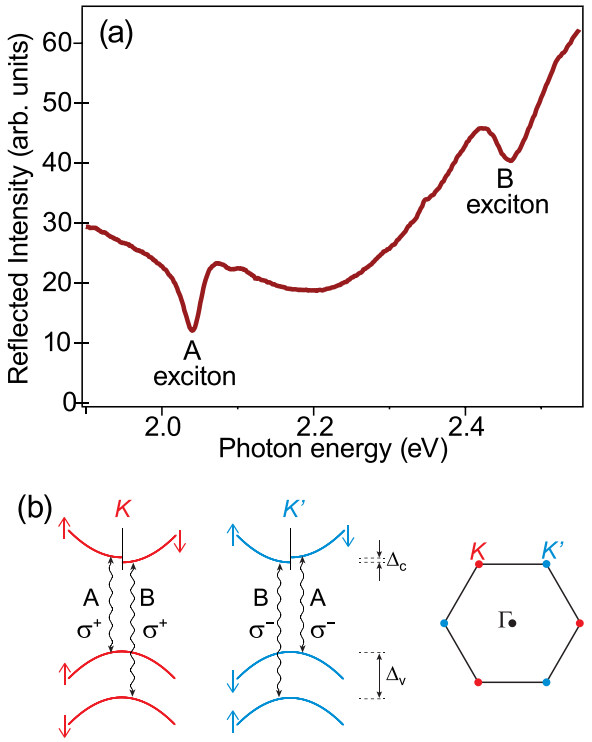

FIG. 2. (Color online) (a) Reflection spectrum from a monolayer WS_2 film at zero magnetic field and at $T = 4$ K. The A and B exciton features are clearly visible on top of a smoothly varying background. (b) Schematic of the conduction and valence bands in the vicinity of the K and K' valleys of monolayer WS_2. The A and B exciton optical transitions (wavy lines) and the associated optical selection rules for circularly polarized σ^+ and σ^- light are indicated. Spin–orbit coupling splits the spin-up and spin-down states in the conduction and valence bands ($\Delta_c \approx 30$ meV, $\Delta_v \approx 400$ meV).

C. Valley Zeeman effect

As described above, we selectively probe transitions in the K or K' valley by using a circular polarizer film (linear polarizer + quarter wave plate) mounted either over the delivery fiber or over the collection fiber. Since it is difficult to switch the position of the polarizer during an experiment (this would require disassembly of the probe and would likely lead to a different spot that is probed on the sample), we typically fix the position of the circular polarizer (e.g., over the delivery fiber), and pulse the magnet in the positive (+65 T) and then in the negative (−65 T) field direction. For nonmagnetic samples, the latter case is in principle equivalent (by time-reversal symmetry) to measuring the σ^- optical transitions in the *positive* field. Nonetheless, we did verify that measurements using both configurations of the circular polarizer gave consistent results, as shown in Fig. 3. Absolute sign conventions were confirmed via magnetoreflectance studies of a diluted magnetic semiconductor ($Zn_{.92}Mn_{.08}Se$), for which $\sigma^\pm$ optical transitions are easily identified in small magnetic fields.

Figure 3 shows circularly polarized magnetoreflection spectra from monolayer WS_2 in pulsed fields to ±60 T using both configurations of the circular polarizing film. The A and B exciton features shift with applied magnetic field and are fit using complex (absorptive + dispersive) Lorentzian lineshapes. The smooth and slowly varying background that is due to the reflection from the Si/SiO_2 substrates [see Fig. 2(a)] does not change with magnetic field (as expected), and is incorporated into the fits as a smooth and field-independent background. Figure 3 shows that the expected symmetry between positive and negative magnetic fields is confirmed (blue and red data traces, respectively). The spectra reveal a well-resolved splitting of the A and B excitons of ~14 meV at 60 T, and the derived g-factors of approximately −4 agree well with our recently published results[19] and are in reasonable agreement with recent reports of the valley Zeeman effect in the monolayer transition-metal diselenides WSe_2 and $MoSe_2$.[11–16]

These measurements (here and in Ref. 19) provide the first experimental values of the valley Zeeman effect of both the A *and* B excitons in monolayer TMD materials. As discussed in detail in Ref. 19, the fact that the measured values of $g \simeq -4$ for *both* A and B excitons is unexpected and surprising, because the reduced masses of these two excitons are expected to be different (and indeed, our data provide strong experimental evidence for a mass difference, as described below).

D. Exciton diamagnetic shift

The use of very large magnetic fields also permits the first observation of the small quadratic *diamagnetic shift* of excitons in these monolayer TMD materials. The exciton diamagnetic shift is a fundamental and very important parameter in semiconductor physics,[1,2,41] because it allows to directly measure the physical size of the exciton—an essential material parameter.

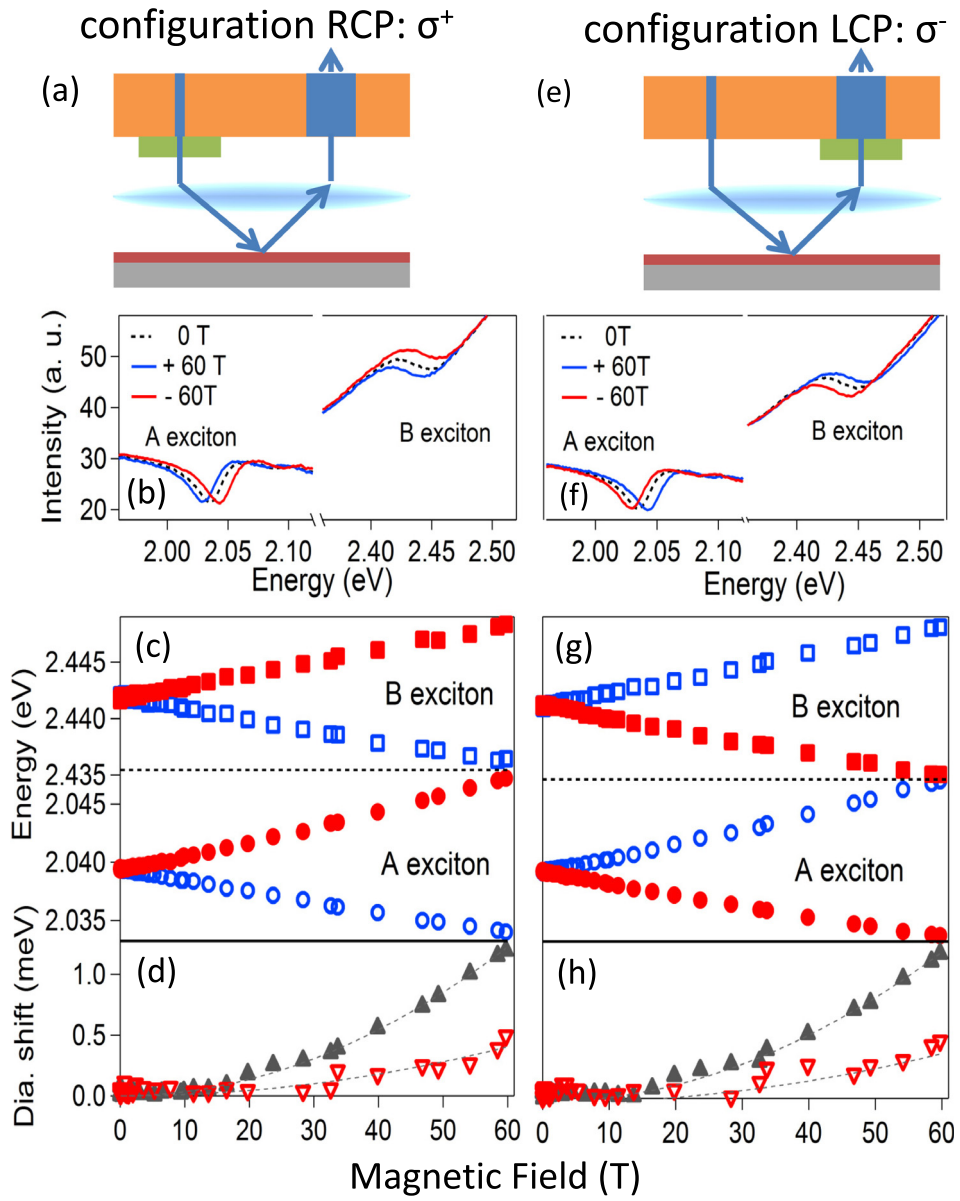

FIG. 3. (Color online) Comparison of the magnetoreflection signals for the two experimental configurations: The circular polarizer film (green) positioned over the delivery fiber, or over the collection fiber, respectively. Dark blue (light red) data are for positive (negative) magnetic fields. Black dashed data are in zero field $T = 4$ K. [(a) and (b)] Magnetoreflection spectra of the A and B excitons for the first configuration. The dark blue trace was acquired at $+60$ T and corresponds to the σ^+ transitions in the K valley. The light red trace at -60 T is equivalent (by time-reversal symmetry) to the σ^- transitions in the K' valley. The valley Zeeman splitting of the optical transitions is clearly visible. (c) Energies of the field-split A and B excitons vs magnetic field. (d) The *average* energy of the field-split exciton peaks reveals the small quadratic diamagnetic shift of the exciton. [(e) and (f)] Similar data and analysis for the second experimental configuration, wherein the circular polarizing film is positioned over the collection fiber.

Independent of the functional form of the Coulomb potential and the resulting shape of the exciton wavefunction,[1,2,41] an exciton's diamagnetic shift ΔE_{dia} is given by

$$\Delta E_{\text{dia}} = \frac{e^2}{8m_r}\langle r^2\rangle B^2 = \sigma B^2, \tag{1}$$

where σ is the diamagnetic shift coefficient, m_r is the exciton reduced mass, r is a radial coordinate in a plane perpendicular to the applied magnetic field B, and $\langle r^2\rangle = \langle\psi_{1s}|(x^2+y^2)|\psi_{1s}\rangle$ is the expectation value of r^2 over the 1s exciton wavefunction $\psi_{1s}(r)$. Equation (1) applies in the "low-field" limit, where ΔE_{dia} and the cyclotron energy $\hbar\omega_c$ are less than the exciton binding energy, which is still very much the case in the monolayer TMDs even at 65 T. Given m_r, σ can then be used to determine the root-mean-square (rms) radius of the 1s exciton in the monolayer plane, r_1

$$r_1 = \sqrt{\langle r^2\rangle_{1s}} = \sqrt{8m_r\sigma}/e. \tag{2}$$

Note that r_1 is not the conventionally defined exciton Bohr radius a_0. The notion of a Bohr radius applies to classic Coulomb potentials that scale as $-1/r$, for which a_0 appears in the functional form of the exciton wavefunction $\psi(r)$. As described below, such conventional potentials likely do not apply to real 2D materials. The rms exciton radius r_1 is a

well-defined parameter for any arbitrary exciton wavefunction (in a conventional bulk material where $V(r) \propto -1/r$, $r_1 = \sqrt{2}a_0$).

To directly reveal ΔE_{dia}, Figs. 3(d) and 3(h) show the *average* exciton energy versus magnetic field. Overall quadratic shifts are observed, indicating diamagnetic coefficients $\sigma_A = 0.32\,\mu\text{eV/T}^2$ for the A exciton and $\sigma_B = 0.11\,\mu\text{eV/T}^2$ for the B exciton (independent of the circular polarizer configuration, as expected). To infer the exciton radius r_1, an exciton reduced mass m_r must be assumed. Theoretical estimates[5,20,44] for the A exciton reduced mass in monolayer WS_2 range from $m_{r,A} = 0.15 - 0.22m_0$, which allow us to directly calculate $r_{1,A} = 1.48 - 1.79\,\text{nm}$ via Eq. (2). These values of r_1 are in reasonable agreement with recent *ab initio* calculations of the 1s exciton wavefunction in monolayer WS_2,[23] and further support a picture of Wannier-type excitons with lateral extent larger than the monolayer thickness (0.6 nm) and spanning several in-plane lattice constants. These results were discussed in detail in Ref. 19.

Temperature-dependent magnetoreflectivity studies were also performed and are shown in Fig. 4. Figures 4(a) and 4(b) show the A and B exciton energies versus magnetic field (for both σ^+ and σ^- polarizations) at different temperatures up to 110 K. The zero-field exciton energies redshift with increasing temperature, as previously reported. The valley Zeeman splitting for the A exciton is largely unchanged with temperature while that for the B exciton slightly increases [Fig. 4(c)]. Importantly, the diamagnetic shift, and therefore the size of the excitons, remains essentially unchanged with increasing temperature [Fig. 4(d)], indicating that the observed temperature-dependent red-shift of the exciton energy is likely due to the reduction of the single-particle bandgap of the material and not to any significant change in the exciton properties.

III. DISCUSSION

Finally, we discuss how knowledge of the exciton diamagnetic shift can also be used to place constraints on estimates of the exciton binding energy—a parameter of significant current interest in the monolayer TMDs, for which both experimental and theoretical estimates vary considerably.[20–30] This procedure was discussed in Ref. 19 for the case of suspended monolayer TMDs, and here, we briefly review these arguments and also present new simulations for the more realistic case of monolayer TMDs on a dielectric substrate.

In contrast to bulk materials, the attractive electrostatic potential $V(r)$ between an electron and hole in 2D materials does not scale simply as $1/r$. This is due the phenomenon of *nonlocal dielectric screening*, wherein the effective dielectric constant that is "seen" by an exciton strongly depends on the electron–hole separation.[25,42–44] Rather, the potential $V(r)$ in a free-standing 2D material in vacuum is believed to assume the following form:

$$V(r) = -\frac{e^2}{8\varepsilon_0 r_0}\left[H_0\left(\frac{r}{r_0}\right) - Y_0\left(\frac{r}{r_0}\right)\right], \tag{3}$$

where H_0 and Y_0 are the Struve function and the Bessel function of the second kind, respectively, and the characteristic length scale r_0 is the screening length $r_0 = 2\pi\chi_{2D}$, where χ_{2D} is the 2D polarizability of the monolayer material. This potential approaches the classic $-1/r$ form at large electron–hole separations ($r \gg r_0$), but diverges only weakly as

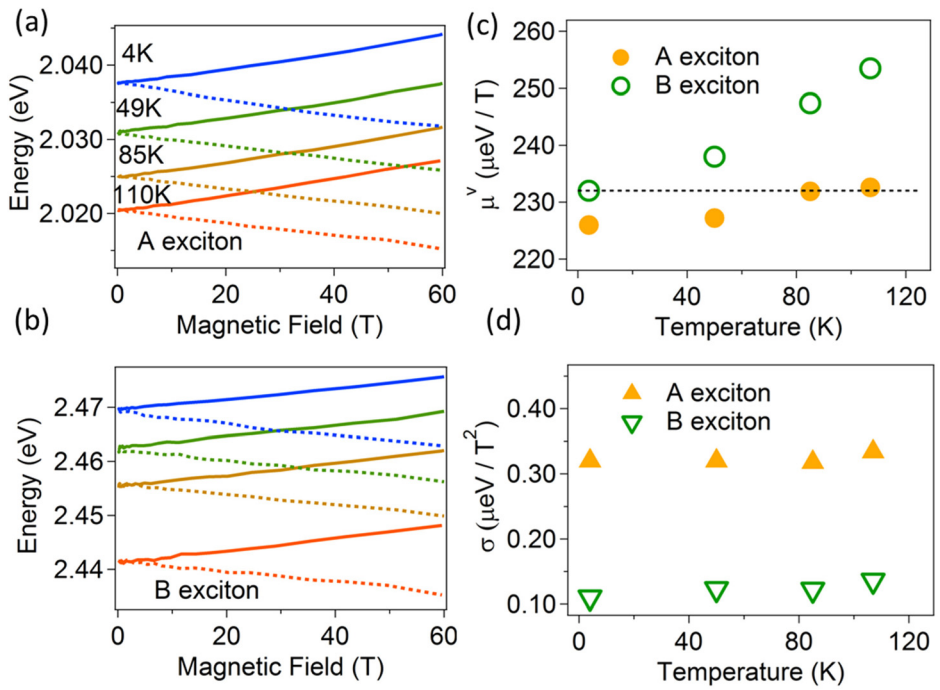

FIG. 4. (Color online) (a) Energy of the A exciton vs magnetic field in monolayer WS_2 for different temperatures. Solid (dashed) lines correspond to positive (negative) magnetic fields. (b) Same, for the B exciton. (c) Valley Zeeman splitting of the A and B excitons vs temperature. (d) Diamagnetic shift of both excitons vs temperature.

log(r) for small r, leading ultimately to a markedly different Rydberg series of exciton states with considerably modified wavefunctions and binding energies.[25,44]

Using this potential, it is possible to numerically calculate via the Schrödinger equation the lowest 1s exciton wavefunction $\psi_{1s}(r)$ and its binding energy for any given reduced mass m_r and screening length r_0. Figure 5(a) shows a color surface plot of the calculated exciton binding energy over a range of possible m_r and r_0. Different colors indicate different binding energies. In addition to the binding energy, the rms exciton radius r_1 and also the expected diamagnetic shift σ were also calculated via Eq. (2) at each (m_r, r_0) point.

Crucially, the solid black lines that are superimposed on this plot indicate *contours of constant diamagnetic shift* that correspond to our experimentally measured values of σ for both the A and B excitons in monolayer WS_2. Therefore, within this model, once a particular reduced mass is assumed, then the value of the exciton binding energy can be uniquely determined by the diamagnetic shift. For example, if the A exciton reduced mass is $m_r = 0.16$ (a common assumption in monolayer WS_2), then the σ_A contour is intercepted at a binding energy of ~410 meV. Moreover, assuming that the dielectric environment and the screening length r_0 are similar for the B exciton, then the parameters for the B exciton are located at the point on the σ_B contour that lies directly to the right of that for the A exciton. This gives a B exciton reduced mass of $0.27m_0$, a radius of 1.16 nm, and a binding energy of 470 meV. The diamagnetic shift is therefore a very useful parameter that can be used to benchmark theoretical calculations of the exciton size and its relation to the exciton binding energy in various 2D materials.

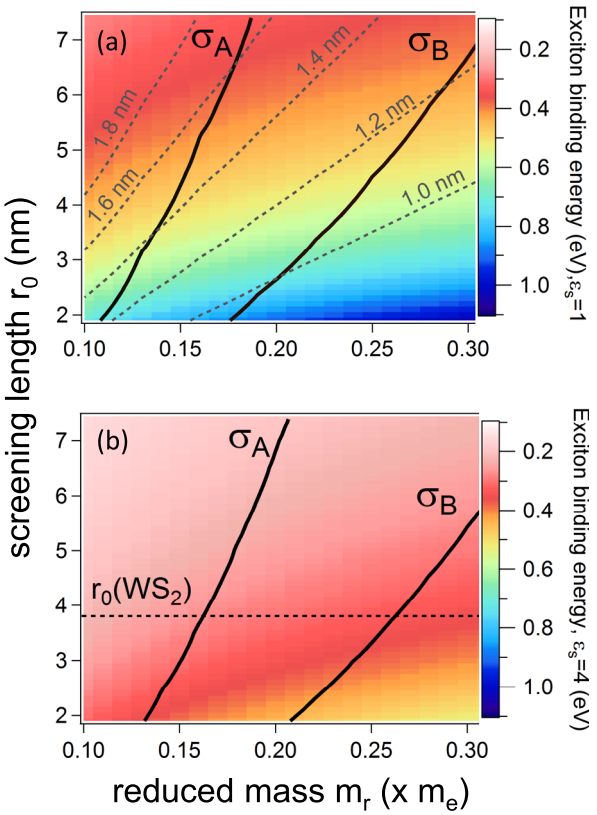

FIG. 5. (Color online) (a) Color surface plot of the calculated 1s exciton binding energy using the nonlocal screening potential $V(r)$ from Eq. (3), over a range of possible reduced masses m_r and screening lengths r_0. This calculation corresponds to the case of a freestanding (suspended) monolayer TMD film in vacuum. Solid black lines indicate contours of constant diamagnetic shift corresponding to that measured for the A and B excitons in monolayer WS_2. Gray dashed lines are contours of constant rms exciton radius r_1. (b) Same, but for the case of a monolayer TMD on a substrate with dielectric constant $\varepsilon_s = 4$, which corresponds approximately to Si/SiO_2 [see Eq. (4)]. The expected screening length r_0 for WS_2 (3.8 nm) is indicated by the dashed horizontal line.

In this paper, we extend these calculations to include the effect of a substrate having dielectric constant ε_s, which is of course a very common experimental situation. The modified potential now assumes the form[25,42–44]

$$V(r) = -\frac{e^2}{8\varepsilon_0 r_0}\left[H_0\left(\frac{(1+\varepsilon_s)r}{2r_0}\right) - Y_0\left(\frac{(1+\varepsilon_s)r}{2r_0}\right)\right]. \quad (4)$$

Figure 5(b) shows the modified surface plot of the exciton binding energy for the case $\varepsilon_s = 4$, which approximately corresponds to the dielectric constant of a SiO_2/Si substrate. For any given (m_r, r_0) pair, the binding energy is reduced as compared to the case of a suspended TMD film where $\varepsilon_s = 1$. Again, assuming that $m_r = 0.16$ for the A exciton, now we find that the binding energy is constrained by the σ_A contour to be ~290 meV, which is near the value reported recently in Ref. 25 (320 meV) but is significantly less than most theoretical predictions and the values of ~700 meV reported from two-photon excitation studies of monolayer WS_2. Importantly, note that in this case where $\varepsilon_s = 4$, the intersection of the σ_A contour with a vertical line representing $m_r = 0.16$ also corresponds quite well to a screening length of $r_0 = 3.8$ nm, which is predicted to be the correct value for monolayer WS_2.[44] A systematic experimental study of the diamagnetic shift as a function of substrate material will shed considerable light on the validity and utility of these numerical models.

In summary, we have described how polarization-resolved optical spectroscopy in very high (pulsed) magnetic fields can reveal new and important parameters of excitons in the recently discovered family of monolayer TMD semiconductors. Owing to the large masses, small exciton radii, and large exciton binding energies in these 2D materials, pulsed magnetic fields have proven to be an invaluable resource. Not only can the Zeeman splitting between the broad absorption lines in the monolayer disulphides (i.e., WS_2 and MoS_2) be clearly resolved—thereby allowing precise measurements of the valley Zeeman effect—but the very small quadratic diamagnetic shift of excitons can now be revealed in these 2D materials for the first time. The importance of diamagnetic shift studies is that it allows direct access to the physical size of the excitons, and further, permits one to constrain estimates of the exciton binding energy. Magneto-optical spectroscopy in pulsed magnetic fields is therefore demonstrated to be a powerful tool for the study and characterization of new 2D materials.

ACKNOWLEDGMENTS

These measurements were performed at the NHMFL, which is supported by the NSF DMR-1157490 and the State

of Florida. Work at NRL was supported by the core programs and the NRL Nanoscience Institute, and by the AFOSR under Contract No. AOARD 14IOA018-134141. Work at Rice University was supported by the AFOSR under FA9550-14-1-0268.

[1]N. Miura, *Physics of Semiconductors in High Magnetic Fields* (Oxford University, Oxford, 2008).
[2]R. S. Knox, *Theory of Excitons* (Academic, New York, 1963).
[3]A. Splendiani, L. Sun, Y. Zhang, T. Li, J. Kim, C. Y. Chim, G. Galli, and F. Wang, Nano Lett. **10**, 1271 (2010).
[4]K. F. Mak, C. Lee, J. Hone, J. Shan, and T. F. Heinz, Phys. Rev. Lett. **105**, 136805 (2010).
[5]D. Xiao, G.-B. Liu, W. Feng, X. Xu, and W. Yao, Phys. Rev. Lett. **108**, 196802 (2012).
[6]X. Xu, W. Yao, D. Xiao, and T. F. Heinz, Nat. Phys. **10**, 343 (2014).
[7]K. F. Mak, K. He, J. Shan, and T. F. Heinz, Nat. Nanotechnol. **7**, 494 (2012).
[8]H. Zeng, J. Dai, W. Yao, D. Xiao, and X. Cui, Nat. Nanotechnol. **7**, 490 (2012).
[9]G. Sallen *et al.*, Phys. Rev. B **86**, 081301(R) (2012).
[10]T. Cao *et al.*, Nat. Commun. **3**, 887 (2012).
[11]D. MacNeill, C. Heikes, K. F. Mak, Z. Anderson, A. Kormányos, V. Zólyomi, J. Park, and D. C. Ralph, Phys. Rev. Lett. **114**, 037401 (2015).
[12]A. Srivastava, M. Sidler, A. V. Allain, D. S. Lembke, A. Kis, and A. Imamoğlu, Nat. Phys. **11**, 141 (2015).
[13]G. Aivazian *et al.*, Nat. Phys. **11**, 148 (2015).
[14]Y. Li *et al.*, Phys. Rev. Lett. **113**, 266804 (2014).
[15]G. Wang, L. Bouet, M. M. Glazov, T. Amand, E. L. Ivchenko, E. Palleau, X. Marie, and B. Urbaszek, 2D Mater. **2**, 034002 (2015).
[16]A. A. Mitioglu, P. Plochocka, Á. Granados del Aguila, P. C. M. Christianen, G. Deligeorgis, S. Anghel, L. Kulyuk, and D. K. Maude, Nano Lett. **15**, 4387 (2015).
[17]L. Yang, N. A. Sinitsyn, W. Chen, J. Yuan, J. Zhang, J. Lou, and S. A. Crooker, Nat. Phys. **11**, 830 (2015).
[18]L. Yang, W. Chen, K. M. McCreary, B. T. Jonker, J. Lou, and S. A. Crooker, Nano Lett. **15**, 8250 (2015).
[19]A. V. Stier, K. M. McCreary, B. T. Jonker, J. Kono, and S. A. Crooker, Nat. Commun. **7**, 10643 (2016).
[20]A. Ramasubramaniam, Phys. Rev. B **86**, 115409 (2012).
[21]H.-P. Komsa and A. V. Krasheninnikov, Phys. Rev. B **86**, 241201 (2012).
[22]G.-B. Liu, W.-Y. Shan, Y. Yao, W. Yao, and D. Xiao, Phys. Rev. B **88**, 085433 (2013).
[23]Z. Ye, T. Cao, K. O'Brien, H. Zhu, X. Yin, Y. Wang, S. G. Louie, and X. Zhang, Nature **513**, 214 (2014).
[24]A. Kormányos, V. Zólyomi, N. D. Drummond, and G. Burkard, Phys. Rev. X **4**, 011034 (2014).
[25]A. Chernikov, T. C. Berkelbach, H. M. Hill, A. Rigosi, Y. Li, O. B. Aslan, D. R. Reichman, M. S. Hybertsen, and T. F. Heinz, Phys. Rev. Lett. **113**, 076802 (2014).
[26]K. He, N. Kumar, L. Zhao, Z. Wang, K. F. Mak, H. Zhao, and J. Shan, Phys. Rev. Lett. **113**, 026803 (2014).
[27]B. Zhu, X. Chen, and X. Cui, Sci. Rep. **5**, 9218 (2015).
[28]G. Wang, X. Marie, I. Gerber, T. Amand, D. Lagarde, L. Bouet, M. Vidal, A. Balocchi, and B. Urbaszek, Phys. Rev. Lett. **114**, 097403 (2015).
[29]T. Stroucken and S. W. Koch, J. Phys. Condens. Matter **27**, 345003 (2015).
[30]A. T. Hanbicki, M. Curriea, G. Kioseogloub, A. L. Friedmana, and B. T. Jonkera, Solid State Commun. **203**, 16 (2015).
[31]K. M. McCreary, A. T. Hanbicki, G. G. Jernigan, J. C. Culbertson, and B. T. Jonker, Sci. Rep. **6**, 19159 (2016).
[32]S. A. Crooker, D. G. Rickel, S. K. Lyo, N. Samarth, and D. D. Awschalom, Phys. Rev. B **60**, R2173 (1999).
[33]S. A. Crooker, E. Johnston-Halperin, D. D. Awschalom, R. Knobel, and N. Samarth, Phys. Rev. B **61**, R16307 (2000).
[34]G. V. Astakhov *et al.*, Phys. Rev. B **71**, 201312 (2005).
[35]K. Alberi, S. A. Crooker, B. Fluegel, D. A. Beaton, A. J. Ptak, and A. Mascarenhas, Phys. Rev. Lett. **110**, 156405 (2013).
[36]E. Johnston-Halperin, D. D. Awschalom, S. A. Crooker, Al. L. Efros, M. Rosen, X. Peng, and A. P. Alivisatos, Phys. Rev. B **63**, 205309 (2001).
[37]M. Furis, J. A. Hollingsworth, V. I. Klimov, and S. A. Crooker, J. Phys. Chem. B **109**, 15332 (2005).
[38]S. Zaric *et al.*, Phys. Rev. Lett. **96**, 016406 (2006).
[39]J. Shaver, S. A. Crooker, J. A. Fagan, E. K. Hobbie, N. Ubrig, O. Portugall, V. Perebeinos, Ph. Avouris, and J. Kono Phys. Rev. B **78**, 081402 (2008).
[40]C. V. Diaconu, E. R. Batista, R. L. Martin, D. L. Smith, B. K. Crone, S. A. Crooker, and D. L. Smith, J. Appl. Phys. **109**, 073513 (2011).
[41]S. N. Walck and T. L. Reinecke, Phys. Rev. B **57**, 9088 (1998).
[42]L. V. Keldysh, JETP Lett. **29**, 658 (1979).
[43]P. Cudazzo, I. V. Tokatly, and A. Rubio, Phys. Rev. B **84**, 085406 (2011).
[44]T. C. Berkelbach, M. S. Hybertsen, and D. R. Reichman, Phys. Rev. B **88**, 045318 (2013).